Poster 1216/SAT019

THE INTERNATIONAL LIVER CONGRESS™

Increased liver content of omega-3-derived lipid autacoids associates with enhanced mitochondrial oxidative phosphorylation, fatty acid β-oxidation and metabolic efficiency

C. LOPEZ-VICARIO [1 2 3], D. SEBASTIAN [4 5], M. CASULLERAS [1 3], M. DURAN-GÜELL [1 3], R. FLORES-COSTA [1 3], F. AGUILAR [3], JJ. LOZANO [2], IW. ZHANG [1 3], E. TITOS [1 2 6], JX. KANG [7], A. ZORZANO [4 5], M. ARITA [8] and J. CLARIA [1 2 3 6].

[1]Biochemistry and Molecular Genetics Service, Hospital Clínic-IDIBAPS, Barcelona, Spain; [2]CIBERehd, Barcelona, Spain; [3]European Foundation for the Study of Chronic Liver Failure (EF Clif) and Grifols Chair, Barcelona, Spain; [4]Institute for Research in Biomedicine (IRB Barcelona), The Barcelona Institute of Science and Technology, Departament de Bioquímica i Biomedicina Molecular, University of Barcelona, Barcelona, Spain; [5]CIBERdem, Barcelona, Spain; [6]Department of Biomedical Sciences, University of Barcelona, Barcelona, Spain; [7]Laboratory of Lipid Medicine and Technology, Massachusetts General Hospital and Harvard Medical School, Boston MA, USA; [8]Laboratory for Metabolomics, RIKEN Center for Integrative Medical Sciences, Yokohama, Japan.

Our data uncover the importance of a lipid membrane composition rich in DHA and its lipid autacoid derivatives to have optimal mitochondrial and metabolic efficiency in the liver.

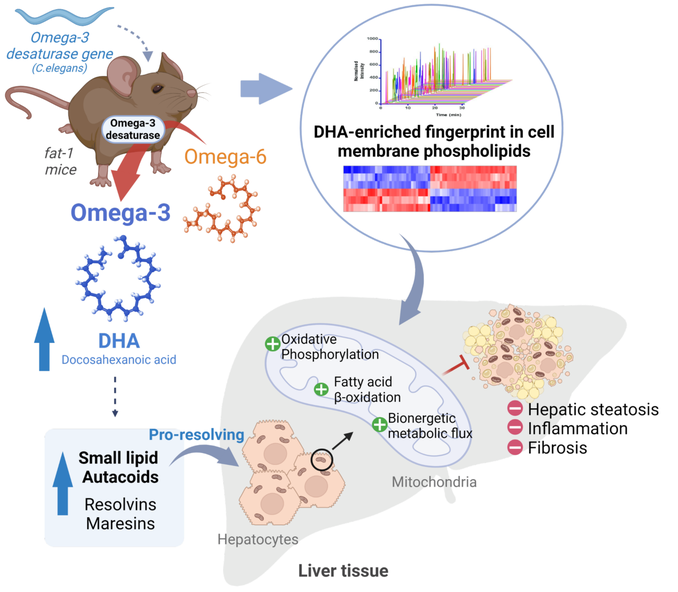

1. Introduction

Mitochondria are the cell powerhouse and are entrusted with the challenging task of providing energy to the cell through the generation of adenosine triphosphate (ATP) (1). Hepatocytes are rich in mitochondria and the liver is a key insulin-sensitive organ coordinating and fine-tuning the complex network(s) of human metabolism (2). At present, there is accumulating evidence that mitochondria are central organelles in the pathogenesis of metabolic dysfunction associated liver disease (3). In fact, defective mitochondrial electron transport chain (ETC) and impaired free fatty acid (FA) β-oxidation (FAO) together with excessive generation of radical oxygen species and lipid peroxidation play a key role in the development of persistent inflammation, increased oxidative stress and extensive liver cell death leading to liver injury and progression to liver fibrosis and, ultimately, to liver cirrhosis (4, 5). Based on these findings, any approach to improve mitochondrial function or to protect hepatocytes from mitochondrial damage is of major relevance for preventing liver-related metabolic dysfunctions.

2 Aim

In the current study we investigated whether changes in the content of essential fatty acid-derived lipid autacoids affect hepatocyte mitochondrial bioenergetics and metabolic flux efficiency.

3 Methods

Chow diet (Chow)
WT n=11
Fat-1 n=9

WT n=33

High-fat diet (HFD)
WT n=13
Fat-1 n=9

Fat-1 n=26

Choline-deficient L-amino acid-defined diet (CDAHFD)
WT n=10
Fat-1 n=8

- Liver mitochondria ultrastructure by transmission electron microscopy (TEM).
- Oxidative phosphorylation by high-resolution respirometry using OROBOROS.
- FAO by radiolabeled [1-14C] oleate oxidation.
- Bioenergetic metabolic fluxes by NADH/$FADH_2$ production.
- Gene and protein expression were determined by real-time PCR and western blot.
- Lipidomic analysis by untargeted and targeted LC-MS/MS.
- Mechanistic studies *in vitro* were performed in hepatocytes exposed to tumor necrosis factor (TNF) α-induced mitochondrial injury.

4. Results

4.1 Distinct liver mitochondrial TEM ultrastructure, expression of OXPHOS and fusion/fission balance in *fat-1* mice.

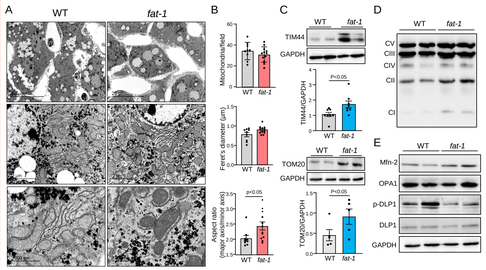

(**A**) Representative electron microscopy (TEM) images of ultrathin liver sections from WT (n=3) and *fat-1* (n=3) mice at magnifications of ×3,000 (upper panels), ×20,000 (medium panels) and ×50,000 (lower panels). (**B**) Number of mitochondria per field, Feret's diameter and aspect ratio (major axis/minor axis) of each mitochondrion. (**C**) Western blot analysis of TIM44, TOM20 and GAPDH in liver tissue from WT (n=8) and *fat-1* (n=8) mice. The densitometry of protein signals normalized to GAPDH are shown below. (**D**) Western blot analysis of OXPHOS complexes I-V in liver tissue from WT and *fat-1* mice. (**E**) Western blot analysis of mitofusin 2 (Mfn-2), Optic Atrophy type 1 (OPA1), phosphorylated and total dynamin like protein-1 (DLP1), and GAPDH in liver tissue from WT and *fat-1* mice.

4.2 Enhanced mitochondrial FAO and energy substrate utilization in *fat-1* mice.

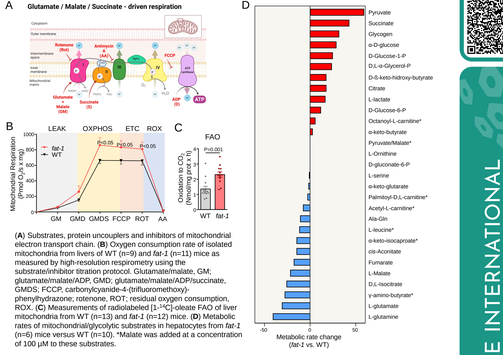

(**A**) Substrates, protein uncouplers and inhibitors of mitochondrial electron transport chain. (**B**) Oxygen consumption rate of isolated mitochondria from livers of WT (n=9) and *fat-1* (n=11) mice as measured by high-resolution respirometry using the substrate/inhibitor titration protocol. Glutamate/malate, GM; glutamate/malate/ADP, GMD; glutamate/malate/ADP/succinate, GMDS; FCCP, carbonylcyanide-4-(trifluoromethoxy)-phenylhydrazone; rotenone, ROT; residual oxygen consumption, ROX. (**C**) Measurements of radiolabeled [1-^{14}C] oleate FAO of liver mitochondria from WT (n=13) and *fat-1* (n=12) mice. (**D**) Metabolic rates of mitochondrial/glycolytic substrates in hepatocytes from *fat-1* (n=6) mice versus WT (n=10). *Malate was added at a concentration of 100 μM to these substrates.

4.3 Identification of a specific DHA-enriched lipid fingerprint in *fat-1* mice.

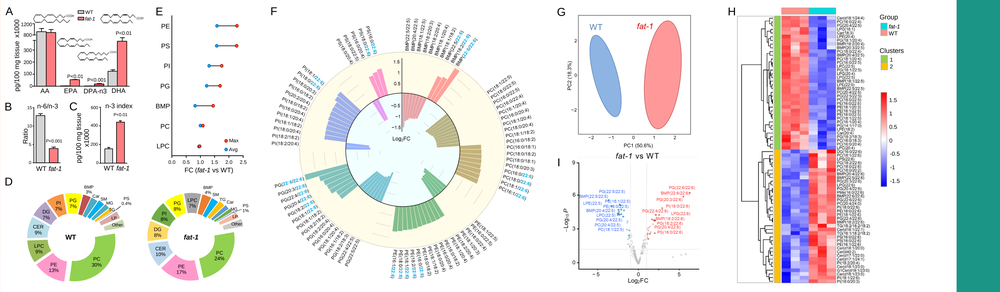

(**A**) Targeted LC-MS/MS analysis of arachidonic acid (AA), eicosapentaenoic acid (EPA), docosapentaenoic acid omega-3 (DPA n-3) and docosahexaenoic acid (DHA) levels in the liver from WT (n=3) and *fat-1* (n=3) mice. (**B**) The hepatic omega-6 (n-6) to omega-3 (n-3)-PUFAs ratio and (**C**) n-3 index are calculated by the total amount of EPA and DHA. (**D**) Pie charts of liver lipid class distribution in WT (n=3) and *fat-1* (n=3) mice as assessed by untargeted LC-MS/MS analysis. (**E**) Lollipop charts of total content of phospholipid subclasses (PE, phosphatidylethanolamines; PS, phosphatidylserines; PI, phosphatidylinositols; PG, phosphatidylglycerols; BMP, bis(monoacylglycero)phosphates; PC, phosphatidylcholines and LPC, lysophosphatidylcholines). (**F**) Circos plot of the fold changes between *fat-1* and WT mice of each individual phospholipid. The presence of DHA (C22:6) is highlighted in blue. Lipid values were log2 transformed before calculating the fold changes between *fat-1* and WT mice. (**G**) Principal component analysis. (**H**) Heatmap of individual lipid species ranked by fold change (up-regulated, red; down-regulated, blue) and significant FDR changes between *fat-1* and WT mice. (**I**) Volcano plot representing the levels of lipid species with the highest positive significant changes (red) and the highest negative significant changes (blue) between *fat-1* and WT mice.

4.4 DHA-derived lipid autacoids protect hepatocytes from TNFα-induced mitochondrial dysfunction

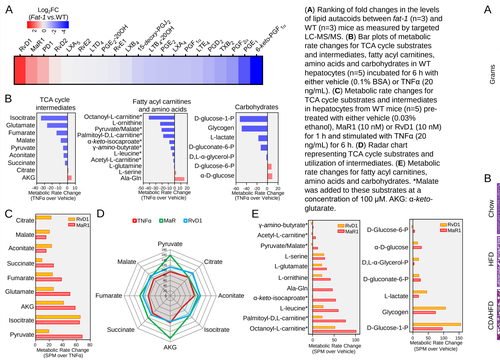

(**A**) Ranking of fold changes in the levels of lipid autacoids between *fat-1* (n=3) and WT (n=3) mice as measured by targeted LC-MS/MS. (**B**) Bar plots of metabolic rate changes for TCA cycle substrates and intermediates, fatty acyl carnitines, amino acids and carbohydrates in WT hepatocytes (n=5) incubated for 6 h with either vehicle (0.1% BSA) or TNFα (20 ng/mL). (**C**) Metabolic rate changes for TCA cycle substrates and intermediates in hepatocytes from WT mice (n=5) pre-treated with either vehicle (0.03% ethanol), MaR1 (10 nM) or RvD1 (10 nM) for 1 h and stimulated with TNFα (20 ng/mL) for 6 h. (**D**) Radar chart representing TCA cycle substrates and utilization of intermediates. (**E**) Metabolic rate changes for fatty acyl carnitines, amino acids and carbohydrates. *Malate was added to these substrates at a concentration of 100 μM. AKG: α-keto-glutarate.

4.5 Liver cells from *fat-1* mice are protected from injury induced by steatogenic and fibrogenic diets

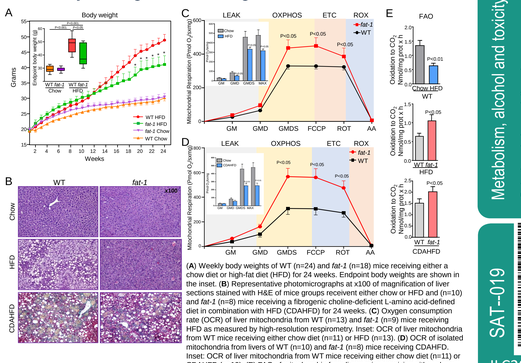

(**A**) Weekly body weights of WT (n=24) and *fat-1* (n=18) mice receiving either a chow diet or high-fat diet (HFD) for 24 weeks. Endpoint body weights are shown in the inset. (**B**) Representative photomicrographs at x100 of magnification of liver sections stained with H&E of mice groups receivent either chow or HFD and (n=10) and *fat-1* (n=8) mice receiving a fibrogenic choline-deficient L-amino acid-defined diet in combination with HFD (CDAHFD) for 24 weeks. (**C**) Oxygen consumption rate (OCR) of liver mitochondria from WT (n=13) and *fat-1* (n=9) mice receiving HFD as measured by high-resolution respirometry. Inset: OCR of liver mitochondria from WT mice receiving either chow diet (n=11) or HFD (n=13). (**D**) OCR of isolated mitochondria from livers of WT (n=10) and *fat-1* (n=8) mice receiving CDAHFD. Inset: OCR of liver mitochondria from WT mice receiving either chow diet (n=11) or CDAHFD (n=10). (**E**) FAO of mitochondria from livers mice receiving either chow diet, HFD or CDAHFD.

5 Conclusions

- This study highlights the critical role of having a tissue environment enriched in omega-3-PUFA to preserve and enhance mitochondrial efficiency in liver cells.
- The omega-3-PUFA derivatives protect liver mitochondria from inflammatory injury and counteract the damaging actions of unresolved inflammation.
- Since mitochondria are central organelles to the pathogenesis of metabolic dysfunction, this study underscores the critical role of maintaining healthy nutritional support with essential fatty acids during the clinical management of this disease.

6 References

1. Scheibye-Knudsen M, et al. *Trends Cell Biol.* 2015;25:158-170.
2. McLaughlin KL, et al. *Sci Rep.* 2020;10:17599.
3. Samuel VT, et al. *Cell Metab.* 2018;27:22-41.
4. Mansouri A, et al. *Gastroenterology*. 2018;155:629-647.
5. Schuster S, et al. *Nat Rev Gastroenterol Hepatol*. 2018;15:349-364.

7 Contact information

Dr. Cristina López-Vicario and Dr. Joan Clària.
Department of Biochemistry and Molecular Genetics, Hospital Clínic Barcelona.
E-mails: clopezv@clinic.cat / jclaria@clinic.cat

DOI: 10.3322/jso.ILC2022.2022

Scan to download the poster

THE INTERNATIONAL LIVER CONGRESS™

Metabolism, alcohol and toxicity
Cristina López-Vicario

SAT–019

ILC2022